Time-Dependent Density Functional Theory Study of $Fe_2(CO)_9$ Low-Lying Electronic Excited States

Luca Bertini, Claudio Greco, Luca De Gioia, and Piercarlo Fantucci*

Department of Biotechnology and Biosciences Universitá degli Studi di Milano-Bicocca Piazza della Scienza, 2, 20126 Milan, Italy

Received: July 20, 2006; In Final Form: September 11, 2006

The valence electronic excited states of $Fe_2(CO)_9$ have been studied using the time-dependent density functional theory (TDDFT). Both tribridged D_{3h} and monobridged C_{2v} structures have been considered, and the structure of selected low-lying singlet and triplet excited states have been optimized on the basis of the TDDFT analytical gradient. Optimized excited-state geometries are used to obtain an insight into certain aspects of the $Fe_2(CO)_9$ photochemistry. The $Fe_2(CO)_9$ (D_{3h}) first triplet and second singlet excited states are unbound with respect to dibridged $Fe_2(CO)_8 + CO$, and the first two monobridged $Fe_2(CO)_9$ (C_{2v}) singlet states are unbound with respect to the $Fe(CO)_5 + Fe(CO)_4$ dissociation. These results are discussed in light of the experimental data available.

1. Introduction

$Fe_2(CO)_9$ was the first homoleptic binuclear transition metal carbonyl ever synthesized[1] and it is still one of the best known and most extensively studied. Cotton et al.[2] established in 1973 by X-ray diffraction that the ground state of $(CO)_3Fe(\mu\text{-}CO)_3Fe(CO)_3$ (see Figure 1a) has D_{3h} symmetry.

Some very important aspects of the reactivity of this complex are of the photochemical type, starting from its preparation through $Fe(CO)_5$ photolysis according to

$$2Fe(CO)_5 \xrightarrow{h\nu} Fe_2(CO)_9 + CO$$

In 1971 Poliakoff and Turner[3] reported on the photochemistry of this binuclear iron carbonyl, showing that $Fe_2(CO)_9$ in matrixes at low temperature (20 K) undergoes CO photolysis under irradiation

$$Fe_2(CO)_9 \xrightarrow{h\nu} Fe_2(CO)_8 + CO$$

The nature of the products depends on the reaction conditions. The initial stage of the photolysis results in the dibridged $Fe_2(CO)_8$ isomer. At a slightly higher temperature (30 K) the system undergoes thermal isomerization, resulting in the unbridged isomer. A detailed study[4] of the changes of the infrared spectra during the reaction demonstrated that the structure of the unbridged isomer of $Fe_2(CO)_8$ is of D_{2h} symmetry.

The aim of the present theoretical study is to investigate the low-lying singlet and triplet excited-state structures of $Fe_2(CO)_9$, obtained by means of geometry optimization using the TDDFT excited-state energy analytic gradients. To the best of our knowledge no similar studies have been previously reported for this complex.

The basic idea of this investigation is to consider $Fe_2(CO)_9$ as a model structure for studying the Fe binuclear complexes with bridged ligands, whose photochemistry has the same common features. For example, the Fe-only hydrogenase active site in its carbon monooxide inhibited form has a two-iron cluster with one μ-CO, a bridged propanedithionate group, two terminal CO, and two CN^- ligands. This system goes through a temperature-dependent light-induced CO dissociation at cryogenic temperature (15 K) very similar to that of $Fe_2(CO)_9$, as pointed out by Chen et al.[5] However, key structure features, such as the positions of the CO ligands around the metal center in the enzyme, are still a matter of debate. The availability of simple model systems such as $Fe_2(CO)_9$ provides the opportunity to obtain insight into such an issue by modeling the possible paths of the photochemical CO dissociation.

Published theoretical studies on $Fe_2(CO)_9$ were mainly devoted to the question of the Fe−Fe bond interaction, which still remain a matter of debate. Although the empirical 18-electron rule predicts the presence of an Fe−Fe bond, molecular orbital (MO) analysis ruled out this hypothesis,[6] emphasizing that the negative Fe−Fe Mulliken overlap population corresponds to an Fe−Fe repulsive instead of attractive character.[7,8]

On the basis of Bader's quantum theory of atoms in molecules (QTAIM),[9] no Fe−Fe bond critical point was found, even if recent[10] computations of Bader's electron delocalization index reveals nonnegligible Fe−Fe interaction.

Besides the question of the Fe−Fe bond, Jang et al.[11] studied the $Fe_2(CO)_9$ molecular structure and the vibrational frequencies at B3LYP level, and Xie et al.[12] performed a comprehensive DFT analysis of the different isomers of $Fe_2(CO)_x$ ($x = 9-6$). Hunstock et al.[13] also studied the electronic structure of the monobridged C_{2v} isomer $(CO)_4Fe(\mu\text{-}CO)Fe(CO)_4$ (Figure 1b). This structure has three groups of equivalent terminal CO groups: one μ-CO, four axial CO perpendicular to the Fe−μ-CO−Fe plane, and two cis-CO and two trans-CO in the Fe−μ-CO−Fe plane. The authors[13] found that this isomer lies 3.3 kcal/mol higher in energy with respect to the D_{3h} form.

The present paper is organized as follows. In the first part the ground-state potential energy surface (PES) is analyzed and the choice of the DFT functional (BP86) is justified on the basis of the comparison of its results for D_{3h} $Fe_2(CO)_9$ optimized geometries, bond energy dissociation, and CO stretching frequencies with the corresponding results of various functionals and experimental values.

* To whom correspondence should be addressed. E-mail: piercarlo.fantucci@unimib.it.

10.1021/jp0646022 CCC: $33.50 © 2006 American Chemical Society
Published on Web 11/04/2006

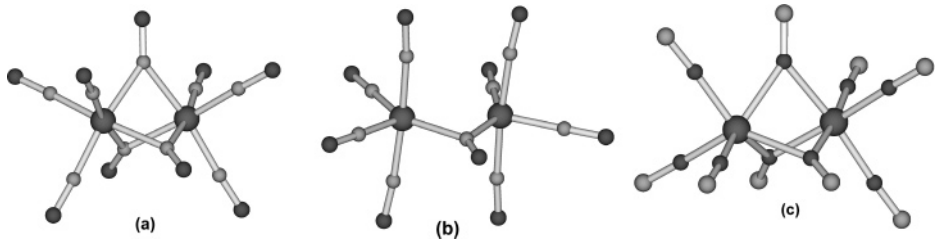

Figure 1. Structure of D_{3h} (a), C_{2v} (b), and C_{3v} (c) $Fe_2(CO)_9$ isomers.

TABLE 1: $Fe_2(CO)_9$ D_{3h} Ground-State DFT Optimized Geometry as a Function of the DFT Functionals versus Experimental Geometries

	exp	BP86	B3LYP	PBE	PBE0
Fe−Fe[a]	2.523	2.523	2.536	2.517	2.479
Fe−C_μ	2.016	2.009	2.014	2.005	1.981
Fe−C	1.838	1.819	1.835	1.820	1.808
C_μ−O	1.176	1.171	1.163	1.173	1.161
C−O	1.152	1.151	1.138	1.152	1.135
Fe−C−O	177.1	177.0	177.6	177.0	177.8
Fe−C_μ−Fe	77.6	77.8	78.0	77.8	77.5
C−Fe−C	96.1	96.0	96.5	95.9	96.8
E_{GS}[b]		−3548.585059	−3547.29986	−3546.54922	−3546.33056
BDE Fe−Fe[c]	29	26.6	10.1	31.5	24.7
BDE Fe−CO	28	29.9	24.6	33.0	34.0
$\nu(a_1')$[d]	2112	2096	2181	2100	2223
$\nu(a_1')$	1891	1904	1960	1909	1994
$\nu(e')$	2016	2027	2112	2032	2154
$\nu(e')$	1814	1878	1919	1883	1953
$\nu(a_2'')$	2088	2053	2131	2058	2172
$\nu(e'')$	1990	2022	2107	2027	2149
sum[e]		171	499	182	743
R^2 [f]		0.959	0.947	0.959	0.943

[a] Bond distances in Å; bond angles in degrees. Experimental values from ref 2. [b] Ground d state energies in hartree. [c] Bond dissociation energies (BDE) in kcal/mol. Experimental values from refs 26 and 27. [d] Stretching CO frequency in cm^{-1}. Experimental values and assignment from refs 39 and 40. [e] Sum $= \sum_i |\nu_{exp,i} - \nu_{computed,i}|$ in cm^{-1}. [f] R^2 is the parameter relative to the linear regression of the function ν_{exp} versus $\nu_{computed}$.

In the second part of the paper the excited-state optimized geometries are taken into account in the context of the photoreactivity of $Fe_2(CO)_9$ complex. The issues addressed here are the CO dissociation paths on the excited-state PES and the possible photochemical role of the C_{2v} monobridged isomer.

2. Computational Methods

In this paper computations are always performed using the pure gradient generalized approximation (GGA) BP86 DFT functional[14,15] because the results obtained are in accordance with experimental values but, above all, because of the opportunity to use the resolution of identity (RI) technique,[16] which is compatible with pure GGA functionals only. RI calculations are highly suited for excited-state geometry optimization, due to the fact that a large number of cycles is needed to fulfill convergence criteria.

Analytic excited-state energy gradients have been recently implemented[19] within the TURBOMOLE[17] suite of programs in combination with the RI[20] technique. Basis sets of triple-ζ plus polarization split valence quality (TZVP hereafter)[18] are adopted for all atoms in the complex. All excited-state geometry optimizations were carried out within C_{2v} symmetry, with convergence criteria fixed to 0.001 hartree·$Å^{-1}$ for the gradient norm vector.

3. Results

3.1. Ground State. The $Fe_2(CO)_9$ PES has the global minimum of D_{3h} symmetry, with three bridged CO and three terminal CO on each metal atom (see Figure 1a). This result has been also theoretically confirmed by other DFT and MP2 studies.[11,13] In particular, Jang et al.[11] found that the B3LYP/DZP level of theory gives optimized geometry in good agreement with the experimental geometry, whereas BP86/DZP underestimates the Fe−Fe and Fe−C and overestimates the C−O distances.

To carefully asses the quality of our BP86 results obtained with the TZVP basis set in comparison to other pure and hybrid functional, we carried out the D_{3h} $Fe_2(CO)_9$ geometry optimization using three additional DFT functionals (B3LYP,[21,22] PBE,[23,24] PBE0[25]). The optimized geometry parameters and the normal-mode frequencies for CO stretching are reported in Table 1.

On average, all bond distances and bond angles are in good concordance with experimental X-ray values, except for PBE0 (and PBE to a smaller extent), which tends to underestimate bond distances, in particularly the Fe−Fe distance. BP86 and B3LPY functionals perform in a very similar way, although BP86 reproduces Fe−Fe and C−O distances better. In any case, the largest deviation between BP86 and B3LYP optimized structural parameters never exceeds 1.3%. The differences between pure GGA (BP86 and PBE) and hybrid functionals (B3LYP and PBE0) are more marked when CO stretching normal-mode frequencies are considered. Pure GGA functionals reproduce the experimental values better than hybrid functionals. We estimated the bond dissociation energies (BDE) of Fe−Fe and Fe−CO bonds. These two values are computed as the energy differences for the following reactions

$$Fe_2(CO)_9\ (D_{3h}) \rightarrow Fe(CO)_5\ (D_{3h}) + Fe(CO)_4\ (C_{2v})$$

$$Fe_2(CO)_9\ (D_{3h}) \rightarrow Fe_2(CO)_8\ (C_s) + CO$$

The comparison among computed values with different functionals clearly shows that BP86 provides a prediction in a very satisfactory agreement with the experimental values.[26] Barckholtz et al.[27] computed these values using BP86 with a basis set of double-ζ quality for C and O atoms, and triple-ζ for Fe atoms. The authors found Fe−Fe BDE equal to 29.5 kcal/mol and the Fe−CO BDE equal to 32.5 kcal/mol. The latter has also been computed by Xie et al.[12] at the B3LYP and BP86 levels with the DZP basis set, obtaining 29.4 and 35.1 kcal/mol, respectively. Among our Fe−Fe or Fe−CO BDE computed values, the BP86 values agree more closely with experimental values. In particular, the increase of the basis set quality improves the Fe−CO BP86 value, whereas the B3LYP Fe−Fe BDE value is strongly underestimated (−65.1%).

The accuracy of the computed CO stretching frequencies has been judged on the basis of the correlation coefficient R^2 between the calculated (ν_{exp}) and observed ($\nu_{computed}$) values and the sum of the absolute error values ($\sum_i|\nu_{exp,i} - \nu_{computed,i}|$). Pure GGA values show the best agreement ($R^2 = 0.96$, sum = 172 cm^{-1} for BP86 and sum = 182 cm^{-1} for PBE). The good agreement of BP86 frequencies is in line with the finding of Neugebauer et al.[28] Our analysis of the performance of DFT functionals cannot be considered exhaustive but seems to support the idea that the use of BP86 may be quite beneficial for $Fe_2(CO)_9$.

The analysis of the Frontier MOs (FMO) (see Figure 2) can help to understand the differences between ground and excited states.

In $Fe_2(CO)_9$ (D_{3h}) the HOMO−1 ($13a_2''$) and HOMO ($12e''$) MOs are dominated by Fe-centered d_{z^2} and d_{xy} orbital antibonding combinations and, therefore, they both have Fe−Fe antibonding character.

The analysis of the low-lying virtual orbital may give good indications in the assigning of the excited state. The LUMO ($17e'$) correspond to π^*_{CO} and contains Fe−C_μ and C_μ−O_μ antibonding orbital combinations. LUMO+1 ($14a_2''$) is almost degenerate with LUMO and is antibonding with respect to either the Fe−Fe or C_μ−O_μ bond. LUMO+2 ($18a_1'$) has a π^*_{CO} character and is mainly localized on the terminal CO groups. Finally, the LUMO+3 ($18e''$) and LUMO+4 ($19e''$) play an important role in the low-lying excited states and have π^*_{CO} character on bridged and terminal CO groups, respectively.

As far as the C_{2v} monobridged isomer is concerned, at the BP86/TZVP level, this structure is a first-order saddle point (imaginary normal-mode frequency equal to i19 cm^{-1}) and its energy is 0.0091 hartree (5.7 kcal/mol) higher than the D_{3h} ground-state energy (see Table 2). At the minimum geometry, the C_{2v} isomer is characterized by an increase of the Fe−Fe distance of 0.221 Å with respect to the D_{3h} isomer. The Fe−C distances of the terminal CO groups are similar in C_{2v} and D_{3h} isomers, but the Fe−C−O angle for axial CO is slightly bent (5.2°) out of linearity. The C_{2v} FMO analysis shows that the HOMO ($29b_2$) and LUMO ($30b_2$) have features similar to those of the corresponding MOs in the D_{3h} isomer, being characterized by Fe−Fe d_{xy} and d_{yz} orbital antibonding combinations, respectively. LUMO+1 ($34a_1$) and LUMO+2 ($15b_1$) MOs have π^*_{COax} and π^*_{COcis} character, whereas LUMO+3 ($16b_1$) is $\pi^*_{COtrans}$. Following the eigenvector associated with the imaginary frequency mode, one can find that this transition state controls the interconversion of two terminal and two bridged CO groups. The mechanism of such interconversion is similar to the Berry pseudorotation of $Fe(CO)_5$, but in $Fe_2(CO)_9$ the energy barrier is much higher (5.7 kcal/mol) than that in $Fe(CO)_5$ (about 1 kcal/mol).

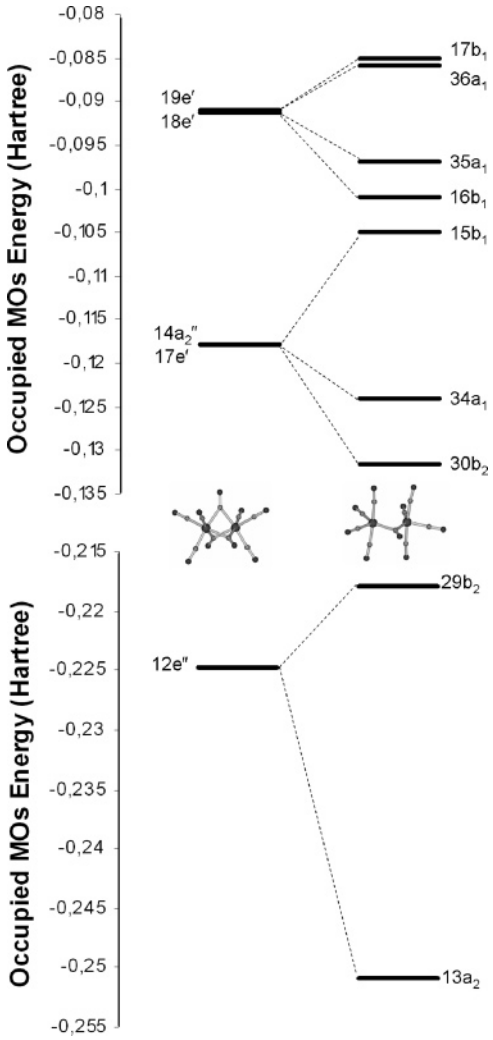

Figure 2. $Fe_2(CO)_9$ ground-state MOs energy diagram: D_{3h} (left) and C_{2v} (right) symmetries.

TABLE 2: BP86/TZVP C_{2v} Monobridged $Fe_2(CO)_9$ Total Energy and Optimized Geometry

	C_{2v}
Fe−Fe[a]	2.734
Fe−C_μ	2.000
Fe−C	1.815
	1.828
	1.782
C_μ−O	1.178
C−O	1.154
	1.156
	1.154
Fe−C−O[a]	174.8
	178.4
	179.0
Fe−C_μ−Fe	86.2
C−Fe−C	112.7
	90.5
	87.9
$E_{1\mu}$[b]	−3548.57595
$E_{1\mu} - E_{3\mu}$[c]	5.7

[a] Bond distances in Å; bond angles in degrees. [b] Energy for the monobridged C_{2v} form $E_{1\mu}$ in hartree. [c] $E_{1\mu} - E_{3\mu}$ is the energy gap in kcal/mol in relation to the tribridged form.

The $D_{3h} \rightarrow C_{2v}$ MO energy correlation diagram is reported in Figure 2. The analysis of FMOs reveals that the HOMO ($29b_2$) and HOMO−1 ($13a_2$) of the C_{2v} form derive from the HOMO of the D_{3h} form. In the C_{2v} form, the HOMO $29b_2$ has

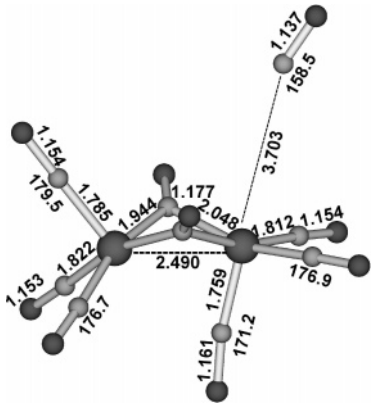

Figure 3. Structure of transition state for the CO terminal dissociation reaction $Fe_2(CO)_9$ (D_{3h}) → $Fe_2(CO)_8$ (C_s) + CO.

Fe−Fe antibonding character and is higher in energy than the D_{3h} HOMO, whereas HOMO−1 $13a_2$ is lower in energy and has Fe−Fe bonding character.

As for the pseudorotation, we found a stationary point corresponding to the 120° rotation of an $Fe(CO)_3$ group, which becomes eclipsed with the three μ-CO groups (see Figure 1c). This C_{3v} structure is higher in energy by 0.0490 hartree (30.7 kcal/mol) and is a third-order saddle point being characterized by imaginary frequencies equal to i140.5, i108.2, and i108.2, respectively.

We then considered the dissociation of one CO ligand through the characterization of the corresponding transition state (TS). Because $Fe_2(CO)_9$ (D_{3h}) has two chemically different CO groups, we have considered both reaction paths corresponding to the dissociation of a terminal or a bridged carbonyl. Let us first consider the dissociation of a terminal CO ligand. The reaction is the following:

$$Fe_2(CO)_9\ (D_{3h}) \rightarrow Fe_2(CO)_8\ (C_s) + CO$$

The structure of the transition state is reported in Figure 3 and its energy is −3548.5371 hartree, 30.1 kcal/mol above the D_{3h} ground state. The reaction mechanism consists of the conversion of a bridging CO into a terminally coordinated CO, followed by the dissociation of a terminal CO in the trans position to the first. In this TS structure, the CO leaving group has an Fe−C distance of 3.703 Å and the $Fe_2(CO)_8$ fragment has an almost exact C_s symmetry, which is close to the global $Fe_2(CO)_8$ BP86 minimum.[31] The optimized BP86/TZVP ground state of the $Fe_2(CO)_8$ (C_s) structure reveals an Fe−Fe distance of 2.488 Å, which is extremely similar to the distance computed for the TS (2.490 Å). It is interesting to note that the barrier of the inverse reaction $Fe_2(CO)_8$ + CO → $Fe_2(CO)_9$ is just 0.5 kcal/mol.[32] Even if we consider this result underestimated, we can certainly conclude that $Fe_2(CO)_8$ is highly unstable, with a strong CO affinity to form $Fe_2(CO)_9$. For the dissociation of a μ-CO, the attempts to find a genuine TS failed. We first found a van der Waals complex in which $Fe_2(CO)_8$ (C_{2v}) loosely binds a CO molecule (Fe−C distances of 6.543 and 6.625 Å with energy equal to −3548.5356 hartree). Several guess structures for the eigenvector-following optimization have been considered, but none of them converged on the desired transition state. Among these structures, the lowest in energy corresponds to the rotation of the leaving μ-CO.[33] The corresponding energy barrier of 0.051 hartree (32.0 kcal/mol) might be considered as an estimate of the true barrier.

The vertical excitation energies of $Fe_2(CO)_9$ in D_{3h} and C_{2v} forms are reported in Table 3. Because in both cases the two Fe atoms lie on the *y*-axes, the correlation of the symmetry species between D_{3h} and C_{2v} point groups is $A_1' \rightarrow A_1$, $A_1'' \rightarrow A_2$, $E' \rightarrow A_1 + B_1$, $A_1'' \rightarrow B_1$, and $A_2'' \rightarrow B_2$, $E'' \rightarrow A_2 + B_2$. Within the D_{3h} group, only the excitations to A_2'' and E' states are dipole allowed. If we consider the possible distortion to the C_{2v} group, A_1, B_1, and B_2 become dipole allowed. For D_{3h} low-lying excited states the main excitations are of two types, $(12e'') \rightarrow (17e', 18e', 19e')$ and $12(e'') \rightarrow (14a_2'')$. In the first three cases, we have a metal to ligand charge transfer (MLCT) state and, in the second, a d → d metal centered excited state. The corresponding C_{2v} excited states have similar characters, because the MOs involved in the main one-electron excitation for the two isomers are roughly conserved. The lowest singlet and triplet excitations are of d → d type.

TABLE 3: Calculated D_{3h} and C_{2v} $Fe_2(CO)_9$ Vertical Excitation Energies, State Composition and Oscillation Strength

D_{3h}	C_{2v}	$E_{vertical}$[a]	leading configuration	*nm*[b]	*f*[c]
$^1A_1'$		−3548.5851			
$1^3A_2''$	B_2	−3548.4942	72.1 $12e'' \rightarrow 17e'$ 16.4 $12e'' \rightarrow 18e'$ 7.8 $12e'' \rightarrow 19e'$	501.2	0.57
$1^3E'$	$A_1 + B_1$	−3548.4873	$12e'' \rightarrow 14a_2''$	466.0	0.63
$1^3E''$	$A_2 + B_2$	−3548.4857	$12e'' \rightarrow 17e'$	458.8	0.0
$1^3A_1''$	A_2	−3548.4837	$12e'' \rightarrow 17e'$	449.6	0.0
$1^1A_1''$	A_2	−3548.4775	$12e'' \rightarrow 17e'$	423.7	0.0
$1^1E''$	$A_2 + B_2$	−3548.4742	$12e'' \rightarrow 17e'$	411.0	0.0
$1^1A_2''$	B_2	−3548.4723	87.3 $12e'' \rightarrow 17e'$ 7.5 $12e'' \rightarrow 18e'$	404.0	0.014
$1^3A_2''$	B_2	−3548.4698	54.6 $12e'' \rightarrow 18e'$ 26.6 $12e'' \rightarrow 17e'$ 8.4 $12e'' \rightarrow 19e'$ 3.3 $11e'' \rightarrow 18e'$	395.1	0.19
$1^1E'$	$A_1 + B_1$	−3548.4673	$12e'' \rightarrow 14a_2''$	387.0	0.031
C_{2v}		$E_{vertical}$	leading configuration	*nm*	*f*
$^1A_1$		−3548.5751			
1^3A_1		−3548.4978	$29b_2 \rightarrow 30b_2$	581.7	0.066
1^3B_2		−3548.4893	$29b_2 \rightarrow 34a_1$	526.1	0.138
1^1A_1		−3548.4803	$29b_2 \rightarrow 30b_2$	476.3	0.0023
2^3B_2		−3548.4784	84.7 $33a_1 \rightarrow 30b_2$ 8.3 $32a_1 \rightarrow 30b_2$	467.1	0.335
1^1B_2		−3548.4756	$29b_2 \rightarrow 34a_1$	453.9	0.0042
2^3A_1		−3548.4675	$28b_2 \rightarrow 30b_2$	420.0	0.0167
1^1A_2		−3548.4610	$29b_2 \rightarrow 15b_1$	396.5	0.0
1^3B_1		−3548.4569	$29b_2 \rightarrow 14a_2$	382.7	0.164
2^1A_2		−3548.4561	$29b_2 \rightarrow 16b_1$	380.2	0.0
2^1B_2		−3548.4514	87.1 $29b_2 \rightarrow 35a_1$ 5.0 $33a_1 \rightarrow 30b_2$	365.8	0.0026
1^1B_1		−3548.4498	$29b_2 \rightarrow 14a_2$	360.8	0.0058

[a] $E_{vertical}$ is the vertical energy in hartree. [b] *nm* is the excitation energy in nm. [c] *f* is the oscillation strength.

3.2. Singlet Excited States. In the previous section we presented a brief analysis of the results obtained from DFT computations using four different functionals, and comparison has been made between calculated and experimental values for the ground state of $Fe_2(CO)_9$.

For excited states, on the contrary, there are no experimental data available, and one cannot rigorously asses the quality of the TDDFT optimized geometries and computed energy differences. Nevertheless, it is worth to demonstrating the extent of variability in the qualitative and quantitative picture of the electronic structures of the excited states as a function of the DFT functional adopted. For this porpose, we carried out the comparison between the tribridged and monobridged optimized structure on the singlet 1^1A_1 PES. The results are reported in

TABLE 4: Tribridged and Monobridged $Fe_2(CO)_9$ (1^1A_1) Excited-State Optimized Geometries as a Function of the DFT Functionals

tribridged	BP86	B3LYP	PBE	PBE0
Fe−Fe[a]	2.689	2.713	2.675	2.639
Fe−C_μ	2.042	2.053	2.053	2.047
	2.060	2.088	2.036	2.016
Fe−C	1.825	1.846	1.812	1.822
	1.815	1.842	1.822	1.818
C_μ−O	1.177	1.170	1.177	1.165
	1.170	1.157	1.171	1.155
C−O	1.154	1.138	1.153	1.137
	1.155	1.140	1.154	1.135
E_{ex}[b]	−3548.4760	−3547.2000	−3546.44087	−3546.22451
Grad[c]	0.0010	0.0008	0.0014	0.0011
$E_{ex} - E_{GS}$[d]	0.109	0.100	0.108	0.106

monobridged	BP86	B3LYP	PBE	PBE0
Fe−Fe	3.364	3.519	3.311	3.336
Fe−C_μ	2.046	2.089	2.036	2.039
C_μ−O	1.181	1.164	1.181	1.161
E_{ex}	−3548.50841	−3547.2318	−3546.47096	−3546.24456
Grad	0.0004	0.0010	0.0002	0.0002
$E_{ex} - E_{GS}$[b]	0.0766	0.0680	0.0783	0.0860
$E_{1\mu} - E_{3\mu}$[d]	−0.0324	−0.0318	−0.0301	−0.0201

[a] Bond distances in Å. [b] E_{ex} and E_{GS} are the excited-state and ground-state energies in hartree. [c] Grad is the norm gradient vector in hartree·Å^{-1}. [d] $E_{1\mu} - E_{3\mu}$ is the energy gap between monobridged and tribridged structures.

Table 4. For all DFT functionals we found the same qualitative picture: the tribridged form is higher in energy with respect to the monobridged form, with elongated Fe−Fe distances compared to that of the ground state. We first point out that in several cases the relative differences for properties computed with different TDDFT schemes are larger than those of DFT for the ground state. The largest difference in the optimized geometry parameters of 5.9% is found for the monobridged Fe−Fe bond distance computed with B3LYP (3.519 Å) and PBE (3.311 Å), whereas for energy differences, we found the largest differences (38%) between the B3LYP and PBE0 tribridged/monobridged energy gap. B3LYP results sometimes differ considerably from those obtained with the other three functionals, in particular for Fe−Fe bond distances and energy differences. In some other cases, hybrid functionals give results different from those obtained with pure GGA functionals, as in the case of C_μ−O_μ bond distances. Our, albeit limited, analysis shows that the TDDFT picture is qualitatively reliable as it seems to be almost independent from the functional adopted. On the contrary, from the quantitative point of view, TDDFT has higher variability in results compared to ground-state DFT. Finally, in this particular case B3LYP performance is less convincing.

In this investigation we explored the PES of the first four low-lying C_{2v} dipole-allowed excited states. Starting from the D_{3h} tribridged structure, these states are $1^1E''$ (1^1B_2), $1^1A_2''$ (2^1B_2), and $1^1E'$ ($1^1A_1 + 1^1B_1$), respectively. Using the D_{3h}/C_{2v} MOs correlation diagram (Figure 2) and Table 3 we established which were the corresponding monobridged singlet excited states. The results are reported in Table 5 (tribridged) and Table 6 (monobridged).

The trend in the energy differences among tribridged and monobridged structures is the following. For 1^1A_1 and 1^1B_1 PES, the monobridged form is lower in energy compared to the tribridged form, and the opposite is true for 1^1B_2. For the C_{2v} 2^1B_2 state, the geometry optimization did not converge to any stationary point. For the tribridged 1^1B_2 optimized structure, the Fe−Fe distance is similar to that of the ground state, but one of the Fe−C_μ distances increases by 0.108 Å (+5.4%), and the corresponding C_μ−O_μ decreases by 0.014 Å (−1.2%). This effect can be rationalized in the light of the FMO analysis presented above: for 1^1B_2, the 17e′ MO is populated, which is characterized by an antibonding Fe−C_μ contribution. For the remaining optimized singlet excited-state geometries, the only interesting change is the small decrease (<1%) of the Fe−Fe distance in the 2^1B_2 state and the larger increase (+6.5%) for both 1^1A_1 and 1^1B_1 states, which turns out to be almost degenerate.

As far as the monobridged structures are concerned, strong deviations of the optimized geometry parameters are found for 1^1A_1 and 1^1B_2 with respect to the ground state. For 1^1A_1 the most important deviations are the Fe−Fe internuclear distance increase (+18.7%) and a smaller increase of the Fe−C_μ distance (+2.3%). For 1^1B_2 we found a decrease in the Fe−C−O_{ax} angle (−6.8%) and an increase in the Fe−C_{ax} distance of 0.048 Å (+2.6%). The 1^1B_1 optimized structure is close to that of the ground state.

When excited-state structures are discussed, it is important to evaluate the lowest singlet or triplet instability matrix eigenvalues.[34,35] When it reaches a negative value during the geometry optimization, TDDFT yields an unphysical negative value of the excitation energy, whereas a value lower than 0.05 is considered critically small. All lowest singlet instability

TABLE 5: Tribridged $Fe_2(CO)_9$ (D_{3h}) Ground- and Excited-State Optimized Geometry at BP86/TZVP Level

D_{3h}[a]	C_{2v}[a]	E_{opt}[b]	Grad[c]	Fe−Fe[d]	Fe−C_μ	C_μ−O_μ	Fe−C	C−O	Fe−C−O
$^1A_1'$	$^1A_1$	−3548.5851		2.523	2.009	1.176	1.838	1.152	177.1
$1^1E''$	1^1B_2	−3548.4878	0.0011	2.529	2.067	1.182	1.813	1.154	175.7
					2.117	1.162	1.801	1.152	177.5
$1^1A_2''$	2^1B_2	−3548.4764	0.0008	2.507	2.056	1.179	1.818	1.153	178.2
					2.064	1.178	1.815	1.153	177.4
$1^1E'$	1^1A_1	−3548.4764	0.001	2.689	2.042	1.177	1.825	1.154	178.5
					2.060	1.170	1.815	1.153	178.2
	1^1B_1	−3548.4760	0.001	2.688	2.040	1.180	1.818	1.154	178.1
					2.054	1.173	1.829	1.155	179.8
$1^3A_2''$	1^3B_2	−3548.5078	0.0009	2.593	2.125	1.164	1.842	1.154	174.6
					2.123	1.164	1.843	1.154	174.7
$1^3E'$	1^3A_1	−3548.4991	0.0005	2.762	2.042	1.180	1.823	1.153	179.1
					2.062	1.176	1.807	1.153	178.2
	1^3B_1	−3548.4990	0.001	2.775	2.053	1.176	1.810	1.153	178.6
					2.034	1.182	1.830	1.153	179.9
$1^3E''$	2^3B_2	−3548.4960	0.0004	2.574	2.111	1.167	1.819	1.155	174.2
					2.111	1.167	1.823	1.155	173.4

[a] D_{3h} and C_{2v} columns report the electonic molecular term of the excited-state according to the D_{3h} and C_{2v} point groups, respectively. [b] Excited-state energy in hartree. [c] Grad is the gradient norm vector in hartree·Å^{-1}. [d] Selected bond distances and bond angles in Å and degrees.

TABLE 6: Monobridged $Fe_2(CO)_9$ (C_{2v}) Ground- and Excited-State Energies and Optimized Geometry at BP86/TZVP Level

C_{2v}[a]	E_{opt}[b]	$E_{1\mu} - E_{3\mu}$[c]	Grad[d]	Fe−Fe[e]	Fe−C_μ	C_μ−O	Fe−C−Fe[e]	Fe−C_{tr}	Fe−C_{cis}	Fe−C_{ax}	Fe−C−O_{ax}
$^1A_1$	−3548.5760	0.0091		2.734	2.000	1.178	86.2	1.828	1.782	1.815	174.8
1^1A_1	−3548.5084	−0.032	0.0004	3.364	2.046	1.181	110.7	1.807	1.809	1.824	175.8
1^1B_2	−3548.4976	−0.021	0.0004	2.652	2.004	1.175	82.8	1.813	1.787	1.863	163.0
1^1B_1	−3548.4619	0.026	0.0008	2.691	1.973	1.177	85.9	1.809	1.853	1.832	174.9
1^3A_1	−3548.5228		0.025	3.450	2.054	1.183	114.2	1.842	1.830	1.831	176.4
1^3B_2	−3548.5164	−0.017	0.0009	2.628	2.152	1.161	75.3	1.821	1.790	1.868	162.1
2^3B_2	−3548.4991	−0.003	0.0003	3.010	2.077	1.174	92.9	1.819	1.804	1.859	167.5
1^3B_1	−3548.4690	0.03	0.0009	2.691	1.979	1.175	85.7	1.868	1.792	1.833	173.5

[a] The C_{2v} column reports the electonic molecular term of the excited state according to the C_{2v} point group. [b] Excited-state energy in hartree. [c] $E_{1\mu} - E_{3\mu}$ is the difference between the mono- ($E_{1\mu}$) and tribridged ($E_{3\mu}$) ground energies. [d] Grad is the gradient norm vector in hartree·Å^{-1}. [e] Selected bond distances and bond angles in Å and degrees.

eigenvalues are larger than 0.10, except for monobridged 1^1A_1 and 1^1B_2 (0.03 and 0.06, respectively). This suggests that these two PES could have dissociative characters.

3.3. Triplet Excited States. The criteria to select the triplet PES is the same used for the singlet ones. We considered the following PES: $^3A_2''$ (1^3B_2), $^3E'$ (1^3A_1 and 1^3B_1), and E″ (2^3B_2). The results of the geometry optimization are reported in Tables 5 (tribridged) and 6 (monobridged).

The deviations of the tribridged optimized triplet structures compared to the ground-state structure are generally larger than those of singlets but follow the same trends. For tribridged 1^3B_2, the Fe−Fe distance increases by 2.8% with respect to the ground state and 2.5% compared to the 1^1B_2 singlet state. Both Fe−C_μ distances increase by 5.8% and the C_μ−O_μ decrease by 1% compared to the ground state, as results of the increased population of the 17e′ MO. The same type of considerations are valid for 2^3B_2. Both 1^3A_1 and 1^3B_1 states are very close in energy, and their optimized geometries are quite similar. The main feature of these structures is a large increase (10%) in the Fe−Fe distance.

For monobridged 1^3A_1, after only a very few geometry optimization cycles, triplet instability occurred. In this case, the reported geometry parameters were those obtained from the last optimization point calculated, just before transition to negative instability eigenvalue. The dissociative character of this structure is documented by the extremely large Fe−Fe distance, but no further discussion can be made for this evolution path.

The monobridged 1^3B_2 optimized triplet structure has a shorter Fe−Fe distance compared to the ground state, and an Fe−C_{ax} elongated distance of 2.9%.

Regarding the triplet instabilities, only tribridged and monobridged 1^3B_2 have critically small lowest eigenvalues (0.041 and 0.021, respectively), whereas the other triplet states considered have corresponding values higher that 0.05.

4. Discussions

4.1. Modeling of $Fe_2(CO)_9$ CO Photolysis. In the previous section we discussed the structural changes after excitation of $Fe_2(CO)_9$, pointing out the main bond length and bond angle variations. We now consider the possible evolution of these structures to propose a possible path for the $Fe_2(CO)_9$ CO photolysis. To be more precise, we are interested in the dissociative paths, i.e., the PES reaction channels that are not bound in relation to the CO group dissociation.

We start the discussion from the tribridged 1^3B_2 excited state. It is known from the literature that the $Fe(CO)_5$ $^3E'$ triplet is not bound with respect to the dissociation to $Fe(CO)_4 + CO$[36−38] and a similar situation could also occur with the $Fe_2(CO)_9$ first triplet PES. Furthermore, the minimum geometry and triplet lowest instability eigenvalue of 1^3B_2 also suggest that this PES might be considered dissociative.

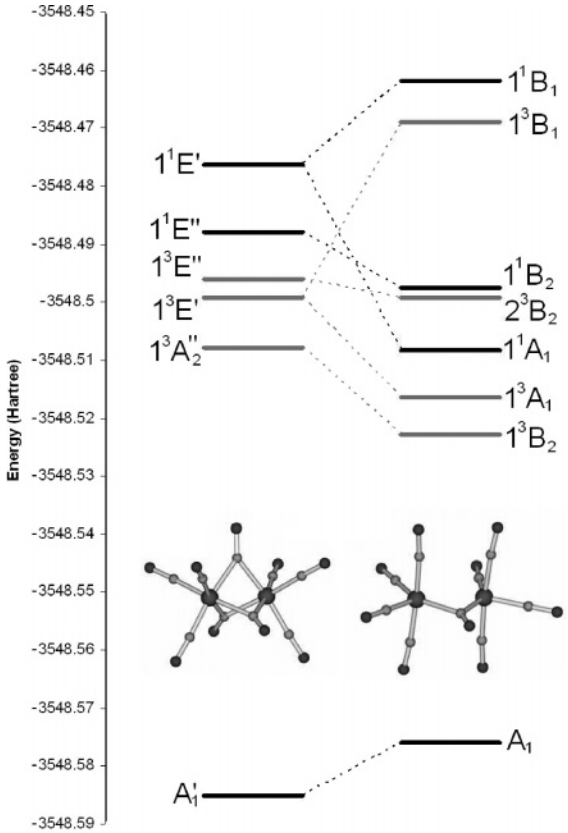

Figure 4. $Fe_2(CO)_9$ ground- and excited-state energy diagram: D_{3h} (left) and C_{2v} (right) symmetries.

To investigate this issue, we optimized the geometry of 1^3B_2 again without any symmetry constraints, starting from the initial ground-state D_{3h} structure. 1^3B_2 results to be unbound compared to the dissociation of a μ-CO group.

$$Fe_2(CO)_9\ (D_{3h},\ 1^3B_2) \rightarrow Fe_2(CO)_8\ (C_{2v}) + CO$$

In Figure 4 the trend of the excited-state energy during the optimization is reported, along with the corresponding ground-state energy. After 18 optimization cycles, the system runs into a negative triplet instability eigenvalue situation: the corresponding structure is plotted in Figure 5.

At variance with the case of the ground state, the $Fe_2(CO)_8$ fragment has C_{2v} symmetry, which represents a second local minimum on the $Fe_2(CO)_8$ BP86 PES, being higher in energy than the C_s form.[31] The Fe−Fe internuclear distance is 2.518 Å, and the CO leaving group has both Fe−C distances equal to 2.366 Å. The Fe−C distances of one of the CO groups in the cis position to the μ-CO are considerably elongated.

The same approach has been applied to 1^1B_2 excited PES which has the same features as 1^3B_2, because both states are

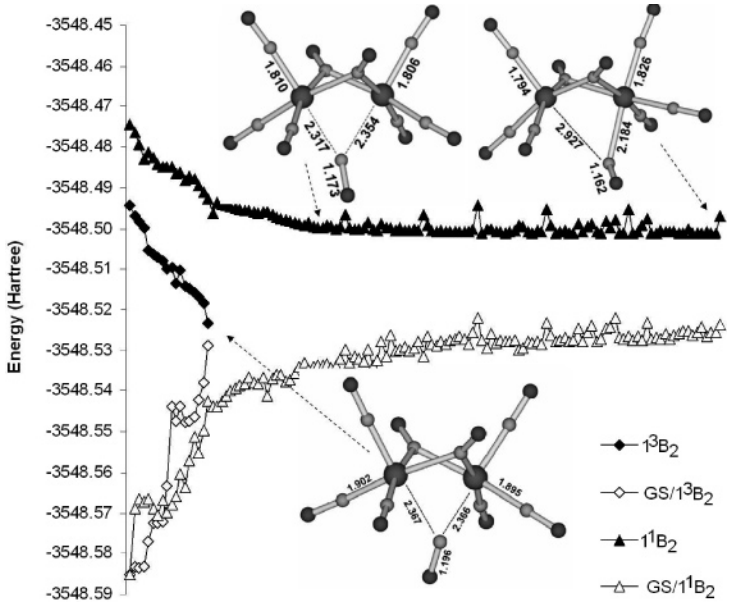

Figure 5. 1^1B_2 and 1^3B_2 excited-state energy evolution during geometry optimization without symmetry constraints. GS/1^1B_2 and GS/1^3B_2 report the ground-state energies at the geometry of the corresponding excited state.

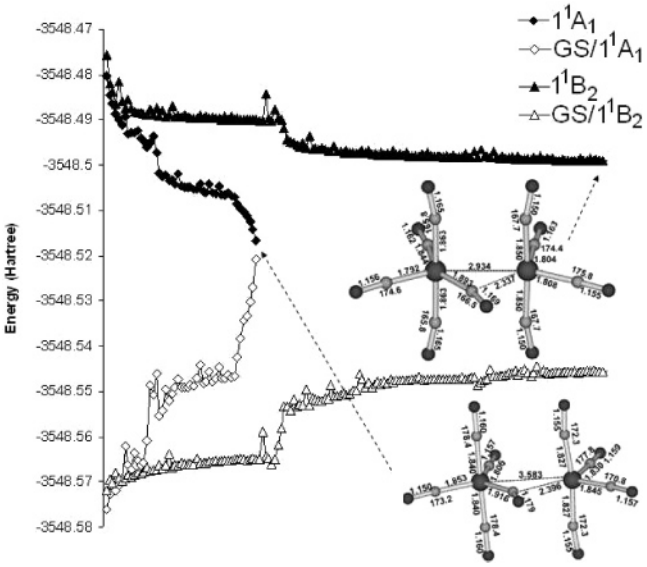

Figure 6. 1^1A_1 and 1^1B_2 monobridged C_{2v} $Fe_2(CO)_9$ excited-state energy evolution during geometry optimization without symmetry constraints. GS/1^1A_1 and GS/1^1B_2 report the ground-state energies at the geometry of the corresponding excited state.

characterized by having the same leading one-electron excitation. In this case no single instability occurs, and the optimization was carried out until the energy variation between two cycles was reduced to about 0.001 hartree (see Figure 5). At this point the geometry optimization was stopped, although the convergence criteria were not met (final gradient norm around 0.05 hartree·Å^{-1}). Indeed, during the last 30 optimization cycles, the geometry fluctuated without further evolution. The two reported structures correspond to those obtained after 60 and 130 optimization cycles.

The first structure is similar to that obtained for 1^3B_2, but the second differs significantly. The leaving μ-CO group approaches one of the Fe atoms, becoming almost a terminal CO group. At the same time the corresponding trans-CO group starts to dissociate (Fe−C increase of 0.2 Å) with a mechanism similar to that found for the ground state. It is worth noting that a similar character for the PES could be found also for the dipole forbidden first singlet state of 1^1A_2 symmetry, because its leading one-electron excitation is equal to that of 1^1B_2 state.

In light of the results obtained we can formulate a mechanism of this CO photolysis. Both 1^1B_2 and 1^3B_2 are photoactive excited states, and they evolve directly to the same products (dibridged $Fe_2(CO)_8$ and CO). The 1^3B_2 channel profile is lower in energy but the transition from the ground state to 1^3B_2 is spin forbidden, although 1^3B_2 could be populated due to the intercrossing from a spin-allowed singlet state through spin−orbit coupling. A more likely possibility is the singlet pathway in which the initial electronic transition is spin and dipole allowed. In both cases we can certainly assess that a bridged isomer of $Fe_2(CO)_8$ is produced. This fact is in qualitative agreement with the experimental findings of Poliakoff et al.,[3] according to which the initial step of the CO photolysis produces only the $Fe_2(CO)_8$ bridged isomer.

4.2. Reaction Paths through C_{2v} Monobridged $Fe_2(CO)_9$ Structure. The analysis of the C_{2v} excited-state optimized geometries clearly demonstrate that the first two singlet and triplet states with A_1 and B_2 symmetries present important deviation from the ground-state geometry. The optimization of the first two singlet excited states 1^1A_1 and 1^1B_2 with no symmetry constraints reveals that the two structures are not bound, and the following dissociation occurs:

$$Fe_2(CO)_9\ (C_{2v},\ 1^1A_1,\ 1^1B_2) \rightarrow Fe(CO)_4 + Fe(CO)_5$$

In Figure 6 we report the energy profile during the geometry optimization for the excited states and the corresponding value of the ground-state energy. As in the case of the D_{3h} 1^3B_2 state discussed above, for 1^1A_1 a negative singlet instability eigenvalue was obtained after 45 cycles. The final structure shows an extremely large Fe−Fe distance (3.583 Å) and the longer Fe−C_μ distance equal to 2.396 Å. In the case of 1^1B_2, we stopped the geometry optimization after 260 cycles. A further geometry optimization results only in an increase of the Fe−Fe distance, with small variations of the geometry parameters within the two fragments. In particular, after the first part of the optimization (from the 20th to 50th cycle) in which the energy was almost constant, we found an abrupt energy drop around the 60th cycle that corresponded to the elongation of

the Fe−Fe distance. The final structures reported in Figure 6 for 1^1B_2 showed the same features as the 1^1A_1 structure (Fe−Fe distance 2.934 Å, Fe−C_μ 2.337 Å).

It is difficult to establish the electronic state of the products of these reactions, because it was not possible to continue the optimization until convergence. For both structures, the $Fe(CO)_4$ fragment has almost C_{2v} symmetry, whereas the $Fe(CO)_5$ fragment has C_s in the first case and C_{2v} symmetry in the second case. We can argue on the basis of these results that monobridged 1^3A_1 structure discussed above could also dissociate in the same way.

These two excited states are involved in the Fe−Fe bond dissociative pathways of $Fe_2(CO)_9$, with the formation of the two mononuclear complexes, but none of them are formed during photolysis, according to Poliakoff and Turner.[3] This fact is in qualitative agreement with the TDDFT picture proposed here. In fact, starting from the D_{3h} form, to populate the C_{2v} 1^1A_1 and 1^1B_2 states, one first needs to populate the D_{3h} 1^1A_1 or 1^1B_2. As we observed in the previous section, D_{3h} $^1B_2$ is unbound with respect to the fragmentation of a μ-CO, and the 1^1A_1 does not have any dissociative character, because the geometry optimization carried out without symmetry constraints leads to the same C_{2v} stationary points.

5. Conclusion and Remarks

The low-lying singlet and triplet excited-state PES of $Fe_2(CO)_9$ have been explored on the basis of the TDDFT analytic gradient computations, with the aim of shedding light on the photochemistry of this system. As a result of a small test on the dependence of DFT results as a function of the functional adopted for the ground-state and 1^1A_1 excited-state computations, the BP86/TZVP level of theory provides better concordance compared to B3LYP. The analysis of the ground-state PES shows the relatively high thermodynamic stability of the $Fe_2(CO)_9$ (D_{3h}) complex. The high barrier of the CO dissociation and the very low barrier of the reverse reaction confirm the experimental observations.

From the analysis of the optimized excited-state geometries we found that tribridged singlet and triplet states of B_2 symmetry are unbound with respect to the dibridged $Fe_2(CO)_8$ form + CO dissociation, in qualitative agreement with experimental findings. In both cases the leading excitation involves the D_{3h} LUMO, which contains Fe−C_μ antibonding orbital combinations.

Finally, monobridged 1^1A_1 and 1^1B_2 singlet states are unbound with respect to the fragmentation into $Fe(CO)_5$ and $Fe(CO)_4$.

This work is encouraging for any future investigation of other organometallic complexes. Soon we plan to investigate the excited states of Fe−hydrogenase biomimetic systems to model the CO photolysis using the information obtained from the $Fe_2(CO)_9$ case.

Furthermore, one of the logical developments of this work is the investigation of the $Fe_2(CO)_8$ excited states, to obtain useful information concerning the Fletcher et al.[4] work regarding the bridged-unbridged photoisomerization. Preliminary geometry optimizations on the $Fe_2(CO)_8$ triplet state at the unrestricted BP86 level, reveal that the unbridged isomers are energetically more stable with respect to the bridged ones.

References and Notes

(1) Dewar, J.; Jones O. *Proc. R. Soc (London)* **1905**, *A76*, 558.
(2) Cotton, F. A.; Troup, J. M. *J. Chem. Soc., Dalton* **1974**, 800.
(3) Poliakoff, M.; Turner, J. J. *J. Chem. Soc. A* **1971**, 1403.
(4) Fletcher, S. C.; Poliakoff, M.; Turner, J. J. *Inorg. Chem.* **1986**, *25*, 3597.
(5) Chen, Z.; Lemon, B.; J.; Huang, S.; Swartz, D. J.; Peters, J. W.; Bagley, K. A. *Biochemistry* **2002**, *41*, 2036.
(6) Summerville, R. H.; Hoffmann, R. *J. Am. Chem. Soc.* **1979**, *101*, 3821.
(7) Bauschlicher, C. W. *J. Chem. Phys.* **1985**, *84*, 872.
(8) Bo, C.; Sarasa, J. P.; Poblet, M. J. *J. Phys. Chem.* **1993**, *97*, 6362.
(9) Corts-Guzmna, F.; Bader, R. F. W. *Coord. Chem. Rev. 249* **2005**, 633
(10) Macchi, P.; Sironi, A. *Coord. Chem. Rev.* **2003**, *238−239*, 383.
(11) Jang, J. H.; Lee, J. G.; Lee, H.; Xie, Y.; Schaefer, F. *J. Phys. Chem. A* **1998**, *102*, 5298.
(12) Xie, Y.; Schaefer, F.; King, R. B. *J. Am. Chem. Soc.* **2000**, *122*, 8746.
(13) Hunstock, E.; Mealli, C.; Calhorda, M. J.; Reinhold, J. *Inorg. Chem.* **1999**, *38*, 5053.
(14) Becke, A. D. *Phys. Rev. A* **1988**, *38*, 3098.
(15) Perdew, J. P. *Phys. Rev. B* **1986**, *33*, 8822.
(16) Eichkorn, K.; Weigend, F.; Treutler, O.; Ahlrichs, R. *Theor. Chem. Acc.* **1997**, *97*, 119.
(17) Ahlrichs, R.; Bar, M.; Haser, M.; Horn, H.; Kolmel, C. *Chem. Phys. Lett.* **1989**, *62*, 165
(18) Schafer, A.; Huber, C.; Ahlrichs, R. *J. Chem. Phys.* **1994**, *100*, 5829.
(19) Furche, F.; Ahlrichs, R. *J. Chem. Phys.* **2002**, *117*, 7433.
(20) Rappoport, D.; Furche, F. *J. Chem. Phys.* **2005**, *122*, 064105.
(21) Lee, C.; Yang, W.; Parr, R. G. *Phys. Rev. B* **1988**, *37*, 785.
(22) Vosko, S.; Wilk, L.; Nussair, M. *Can. J. Phys.* **1980**, *58*, 1200.
(23) Perdew, J. P.; Burke, K.; Ernzerhof, M. *Phys. Rev. Lett.* **1996**, *77*, 3865.
(24) Perdew, J. P.; Burke, K.; Ernzerhof, M. *Phys. Rev. Lett.* **1997**, *78*, 1396.
(25) Adamo, C.; Scuseria, G.; Barone, V. *J. Chem. Phys.* **1999**, *111*, 2889.
(26) Baev, A. K. *Russ. J. Chem.* **1980**, *54*, 1.
(27) Barckholtz, T. A.; Bursten, B. E. *J. Organomet. Chem.* **2000**, *596*, 212.
(28) Neugebauer, J.; Hess, B. A. *J. Chem. Phys.* **2003**, *118*, 7215.
(29) Full, J.; Gonzalez, L.; Daniel, C. *J. Phys. Chem. A* **2001**, *105*, 184.
(30) Harvey, J. N.; Aschi, M. *Faraday Discuss.* **2003**, *126*, 129.
(31) Jacobsen, H.; Ziegler, T. *J. Am. Chem. Soc.* **1996**, *118*, 4631.
(32) The ground-state energy at BP86/TZVP level of theory of $Fe_2(CO)_8$ (C_s) at its minimum geometry is 3435.1775 hartree; the isolated CO molecule at its minimum energy C−O distance of 1.138 Å is −113.3601 hartre.
(33) The energy of this transition state is −3548.5341 hartree with one imaginary frequency of i21.4 cm^{-1}. The Fe−C distances are both 4.215 Å, with a dihedral angle between the Fe−Fe−C_μ and Fe−C_μ-O_μ planes of 90.6°.
(34) Weiss, H.; Ahlrichs, R.; Haser, M. *J. Chem. Phys.* **1993**, *99*, 1262.
(35) Bauernschmitt, R.; Ahlrichs, R. *J. Chem. Phys.* **1996**, *104*, 9047.
(36) Daniel, C.; Benard, M.; Dedieu, A.; Wiest, R.; Veiller, A. *J. Phys. Chem.* **1984**, *88*, 4805.
(37) Ihee, H.; Cao, J. Zewail, A. H. *Angew. Chem., Int. Ed.* **2001**, *40*, 1532.
(38) Poliakoff, M.; Turner, J. J. *Angew. Chem., Int. Ed.* **2001**, *40*, 2809.
(39) Butler, I. S.; Kishner, S.; Plowman, K. R. *J. Mol. Struct.* **1978**, *43*, 9.
(40) Adams, D. M.; Taylor, I. D. *J. Chem. Soc., Faraday Trans. 2* **1982**, *78*, 1551.